Contact Mechanics and Friction on Novel Linear-Motion Bearing with Helical Insert

Nicholas Lambrache*, Mircea – Iulian Nistor, Nicolae Alexandrescu****

** Alef Photonics, Ottawa, Canada, e-mail: Nicholas.Lambrache@alefphotonics.com*
*** Politehnica University of Bucharest, Dept. of Mechatronics, Bucharest, e-mail: mircea.nistor@upb*

Abstract: Helical inserts provide convenient service on low-friction linear-motion bearings. However, effective design requires a better understanding of contact mechanics and friction phenomena involved in the functioning of such bearings. The authors assume predominantly elastic contacts between the elements of the bearing, analyze the local deformations and pressure distribution and discuss experimental solutions for the evaluation of the friction coefficient in such bearings.

Keywords: Linear-Motion Bearings, Contact Mechanics, Translational Friction.

1. INTRODUCTION

Low-friction and convenient service linear-motion bearing with coil inserts have been demonstrated world-wide [1]. A basic configuration of helical insert bearing is represented in fig. 1.

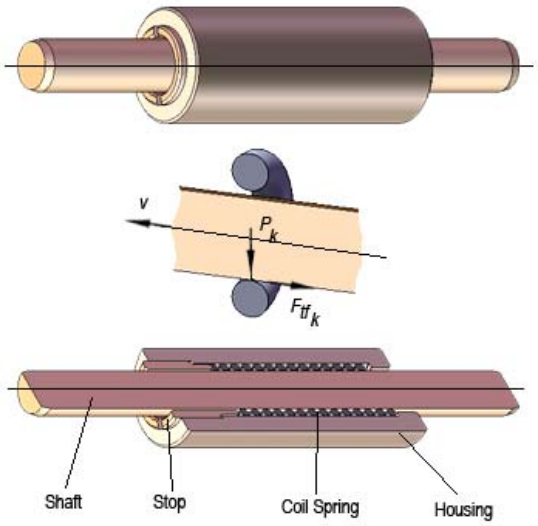

Fig. 1. Linear-motion bearing with helical insert

Helical springs change their outer diameter during deflection and the maximum increase in diameter for a deflection to solid height is [2]:

$$\Delta D_{\max} = 0.05\frac{p^2 - d^2}{D} \qquad (01)$$

In equation (01) d represents the diameter of the wire, D represents the mean diameter and p the pitch of the unloaded helical spring. The end surface of the stop represented in fig. 1 compresses the spring until its coils are touching the housing, and the system spring–housing becomes stiff. The inside diameter of the housing D_{hi} must satisfy the requirement:

$$D_f < D_{hi} < D_u \qquad (02)$$

D_f and D_{sh} are the diameters of the unloaded and respectively deflected to solid height helical spring and $\Delta D_{\max} = D_f - D_{sh}$.

2. CONTACT MECHANICS IN HELICAL BEARINGS

Small loads and low friction characterise linear-motion bearings with helical inserts. Under static conditions and assuming the surfaces in contact are smooth, the elastic limits of materials in contact are not exceeded, the spring and shaft are linearly elastic and isotropic, and localized Hertzian stresses develop as the two surfaces in contact deform under normal loads. The deformations are dependant of the geometry of surfaces in touch, their modulus of elasticity, and the applied normal load [3].

Torus-cylinder contacts are specific to linear-motion bearings with helical inserts. Both solids involved in contact can be described by quadratic surfaces and, according to Hertzian contact theory, an elliptical contact surfaces supporting ellipsoidal distribution of pressures should result under static loads. However, if the centre-line of the cylinder is aligned with the centre-line of the torus, the resulting contact is a *Goodman banana-shaped* surface under normal loads. This effect can be investigated only numerically and Truman, Hills and Sackfield proposed the solution described in [4].

Analytical solutions to the Hertzian problem are possible by approximating the cylinder-torus with a cylinder-cylinder

contact. The diameters of the cylinders are unequal and their axes cross at the coil angle.

For the most general case of quadratic surfaces in contact under a concentrated load P, the area of contact is bounded by an ellipse $x^2/a^2 + y^2/b^2 = 1$, where a and b are the semi-axes of the ellipse. The pressure distribution over the elliptical area of contact is described by [5]:

$$p(x,y) = p_0\left(1-\frac{x^2}{a^2}-\frac{y^2}{b^2}\right)^{\frac{1}{2}} = \frac{3P}{2\pi ab}\left(1-\frac{x^2}{a^2}-\frac{y^2}{b^2}\right)^{\frac{1}{2}} \quad (03)$$

The compression equations are:

$$\delta = \frac{3P(V_1+V_2)}{4}\int_0^{\infty}\frac{d\varphi}{\left((a^2+\varphi)(b^2+\varphi)\varphi\right)^{\frac{1}{2}}} \quad (04)$$

$$A = \frac{3P(V_1+V_2)}{4}\int_0^{\infty}\frac{d\varphi}{(a^2+\varphi)\left((a^2+\varphi)(b^2+\varphi)\varphi\right)^{\frac{1}{2}}} \quad (05)$$

$$B = \frac{3P(V_1+V_2)}{4}\int_0^{\infty}\frac{d\varphi}{(b^2+\varphi)\left((a^2+\varphi)(b^2+\varphi)\varphi\right)^{\frac{1}{2}}} \quad (06)$$

$$V_1 = \frac{1-\nu_1^2}{\pi E_1} \quad (07)$$

$$V_2 = \frac{1-\nu_2^2}{\pi E_2} \quad (08)$$

The semi-axes a and b of the ellipse are generally unknown and are usually determined from known values of A and B. E_1, E_2, ν_1, and ν_2 from equations (07) and (08) represent the Young's moduli of elasticity, respectively the Poisson's ratio of the materials of bodies involved in contact. Let us first consider the contact between two cylinders of radii R_s and R_t with their axes at right angles. For this case [5]:

$$A = \frac{1}{2R_s},\ B = \frac{1}{2R_t} \quad (09)$$

Equations (04), (05) and (06) can be expressed in terms of the eccentricity e of the ellipse of contact using:

$$e = \left(1-\frac{b^2}{a^2}\right)^{\frac{1}{2}} \quad (10)$$

The same equations can be expressed in terms of complete elliptic integral of the first and second class with the changes of variable $\varphi/a^2 = \tau$ and $\tau = \cot^2\theta$. τ goes from 0 to ∞ as θ goes from $\pi/2$ to 0, and $d\tau = -2\cot\theta\csc^2\theta d\theta$ [5].

The complete elliptic integral of the first class K in Legendre form and its derivative are [6]:

$$K = \int_0^{\pi/2}\frac{d\theta}{\left(1-e^2\sin^2\theta\right)^{3/2}} \quad (11)$$

$$\frac{dK}{de} = e\int_0^{\pi/2}\frac{\sin^2\theta d\theta}{\left(1-e^2\sin^2\theta\right)^{3/2}} \quad (12)$$

The complete elliptic integral of the second class E in Legendre form (not to be confused with the Young's moduli mentioned before) and its derivative are [6]:

$$E = \int_0^{\pi/2}\left(1-e^2\sin^2\theta\right)^{1/2}d\theta \quad (13)$$

$$\frac{dE}{d\theta} = -e\int_0^{\pi/2}\frac{\sin^2\theta}{\left(1-e^2\sin^2\theta\right)^{1/2}}d\theta \quad (14)$$

Equations (04), (05) and (06) can be therefore written in terms of the complete elliptic integrals K and E:

$$Aa^3 = -\frac{2QP}{e}\cdot\frac{dE}{de} \quad (15)$$

$$Ba^3 = \frac{2QP}{e}\cdot\frac{dK}{de} \quad (16)$$

$$\delta = \frac{2QP}{a}\cdot K \quad (17)$$

$$Q = \frac{3}{4}(V_1+V_2) \quad (18)$$

Equations (15), (16) and (17) can be combined to provide a compression equation independent of a:

$$\delta = 2K(QP)^{\frac{2}{3}}\left(\frac{1}{R_s\left(-\frac{1}{e}\frac{dE}{de}\right)}\right)^{\frac{1}{3}} \quad (19)$$

The equations connecting the complete elliptic integrals K and E are:

$$\frac{dE}{de} = \frac{1}{e}(E-K) \quad (20)$$

$$\frac{dK}{de} = \frac{1}{e\left(1-e^2\right)}\cdot\left(E-\left(1-e^2\right)K\right) \quad (21)$$

From (20) and (21) one can obtain:

$$-\frac{1}{e}\frac{dE}{de} = \frac{1}{e^2}(K-E) \quad (22)$$

$$\frac{A}{B} = \frac{-\frac{dE}{de}}{\frac{dK}{de}} = \frac{\left(1-e^2\right)(K-E)}{E-\left(1-e^2\right)K} \quad (23)$$

The approximation (28) has a substantial drawback: the characteristic is discontinuous at $v=0$, which creates considerable computational difficulties. There are numerous models of translational friction without this discontinuity. The friction force-relative velocity characteristic of this approximation is shown in Fig. 3. The discontinuity is eliminated by introducing a small and finite region in the zero velocity vicinity, within which friction force is assumed to be linearly proportional to velocity, with the proportionality coefficient F_b/v_{th}, where v_{th} is the velocity threshold. It has been proven experimentally that the velocity threshold in the range between 10^{-4} and 10^{-6} m/s is a good compromise between the accuracy and computational effectiveness [7]. The translational friction force computed with this approximation does not actually stop relative motion when acting forces drop below breakaway friction level. The bodies will creep relative to each other at a very small velocity proportional to acting force. As a result of introducing the velocity threshold, the translational friction equation is slightly modified:

- If $|v| \geq v_{th}$,

$$F=\left(F_C+\left(F_{Brk}-F_C\right)\cdot\exp\left(-c_v|v|\right)\right)\cdot sign(v)+f\cdot v \qquad (29)$$

- If $|v| < v_{th}$,

$$F=v\cdot\frac{\left(fv_{th}+\left(F_C+\left(F_{brk}-F_C\right)\cdot\exp\left(-c_v v_{th}\right)\right)\right)}{v_{th}} \qquad (30)$$

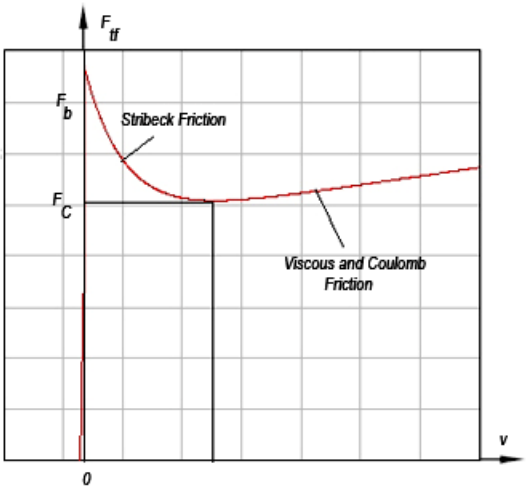

Fig. 3. Continuous translational friction model

The evaluation of the static friction coefficient in linear-motion bearings with helical insert requires high-accuracy experimental approaches. In a typical configuration developed by the authors of this paper, the bearing is placed on a ramp with adjustable angle τ, as shown in Fig. 4. The shaft is connected to a digital force gauge acting vertically with a string guided by a pulley. The force gauge –Imada ZP-5N - records and zooms in to analyze data with Imada ZP Recorder software. The force gauge and the adjustable ramp with the bearing under evaluation are placed on a high capacity hand wheel test stand – Imada HV-500. The stand, force gauge and a screenshot of the recording process are represented in Fig. 5.

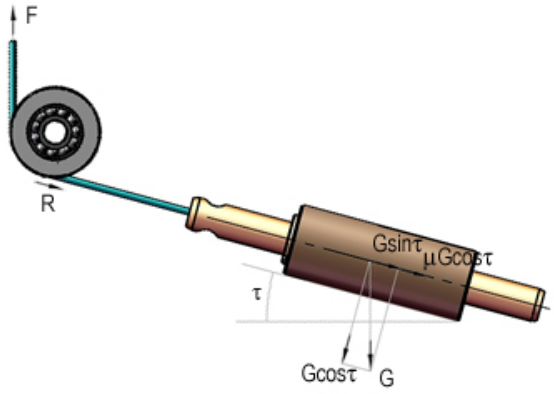

Fig. 4. Schematic of experimental setup for evaluating the static friction coefficient. Imada stand and digital gauge are not shown.

Fig. 5. Imada stand, digital gauges and recorder screenshot. Adjustable ramp is not shown.

For static conditions the force F_τ evaluated by the digital gauge is:

$$F_\tau = G\left(\mu\cos\tau + G\sin\tau\right) + R_\tau \qquad (31)$$